13th World Conference on Earthquake Engineering
Vancouver, B.C., Canada
August 1-6, 2004
Paper No. 340

MODEL TEST AND ENERGY ANALYSIS ON LATERAL FLOW BY WATER FILMEFFECT IN LIQUEFIED SAND SLOPE INCLUDING SILT SEAM

Kazuhiro KABASAWA[1], Takaji KOKUSHO[2] and Aiko SHIMIZU[3]

SUMMARY

Considering that water films formed beneath low permeable layers in liquefied sand have a great influence on lateral flow mechanism, shaking table tests for saturated sand slopes are carried out. In a saturated uniform sand, flow deformation occurs almost exclusively during shaking, while in a sand slope with a sandwiched silt seam, flow deformation in the upper layer occurs after the end of shaking by the water film effect. Results of energy analysis during the post-shaking flow reveal that the shear strength exhibited along the slip surface passing through the water film decreases to 12 % of that of uniform sand. It takes non-zero value presumably due to the roughness of the water film boundary.

Key Words: liquefaction, ground failures, water film, energy analysis

INTRODUCTION

There are quite a few damage reports on the lateral flow in liquefied ground in past earthquakes. In some cases, lateral flow occurred not only during but also after earthquakes and flowed more than a few meters even though in very gentle slopes [1], [2]. In previous researches, lateral flow mechanism was investigated only on homogeneous sand. But they couldn't explain large lateral flow occurred in a gentle slope or after the end of earthquake shaking [3], [4], [5]. Generally, ground is structured by many layers whose permeability is different to each layer. While ground recovers from liquefaction, sedimentation begins in each sublayer. In this process, drained excess pore water may accumulate under a low

---

1. Ph.D. student, Chuo University, Tokyo, Japan, Email: kazuhiro@civil.chuo-u.ac.jp
2. Professor, ditto
3. Master student, ditto

permeability sublayer. We have named this phenomenon as “water film effect”. If the water film is formed continuously along the sublayer, the shear resistance along it reduces, having a great influence on lateral flow mechanism [6]. In this study, in order to make clear the water film effect on flow failure, 1G model shake table tests have been carried out on a saturated sand slope sandwiching a low permeability seam in it parallel to sand slope. The flow mechanism involving water films is discussed from a viewpoint of volume change characteristics of sand observed by CCD cameras. Based on the test results, the internal friction angle exhibited during the post-shaking flow along the water film is attempted to evaluate.

MODEL TEST ON LATERAL FLOW IN SLOPING GROUND WITH A SILT SEAM

A rectangular lucite soil box with a section of 800mm height, 1100mm width and 600mm thickness is filled with water, and fine sand is poured to make a saturated loose sand slope. A silt seam is sandwiched in it in parallel with the slope surface as shown in Fig.1. The thickness of the silt seam is 6mm on average. The grain size curves for the fine sand and the silt are available in Fig.2. Their permeability coefficients are 2×10^{-2} cm/s and 2×10^{-4} cm/s, respectively. The model is liquefied by 3 cycles of cyclic motion in 3Hz. The direction of shaking is perpendicular to the sloping direction as shown in Fig.1 so that the effect of the inertia force be excluded in the lateral flow deformation. In these tests, failure modes are visualized by movements of marker grids made from Japanese noodles attached to the transparent wall of the soil box. Test conditions are shown in Table 1. The tests of uniform sand are also carried out to compare with those of non-uniform sand sandwiching a silt seam.

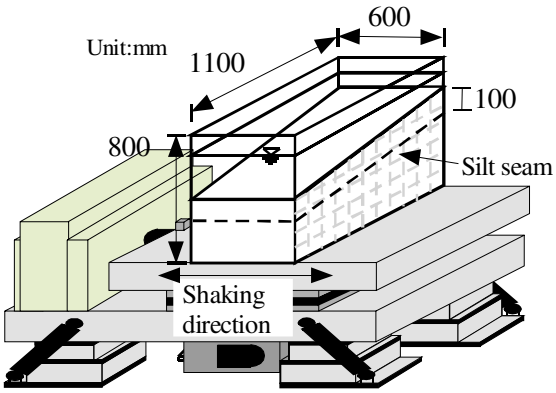

Fig.1 Two dimensional model for saturated sand slope with a silt seam in a lucite box on a shaking table.

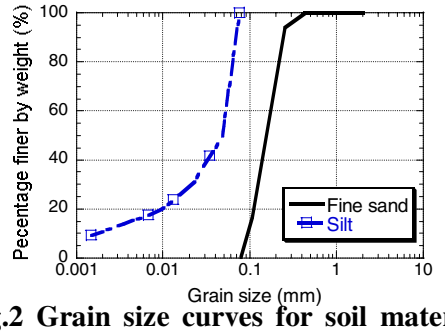

Fig.2 Grain size curves for soil materials used in the tests.

Table 1 Test conditions.

	case1	case2	case3	case4	case5
Impermeable layer	uniform	silt	silt	uniform	silt
Effect of boundary	exist	exist	removed	removed	removed
Slope gradient (%)	24	23	24	5	5
Relative density (%)	27	25	30	39	34
Maximum acceleration (gal)	290	290	280	160	165

In Case3-5, the front and back portions of the sand layer above the silt seam are truncated to remove the confinement effect by the soil container wall, allowing freer flow of the soil mass.

In Fig.3, the deformations of the sand slope during and after shaking are illustrated in two separate charts for Case1 and Case2, respectively. In Case1 without a silt seam, the amount of deformation is very little and the slope deforms continuously mostly during shaking. On the other hand in Case2 with a silt seam, the slope deforms discontinuously after the end of shaking along the silt seam because a water film is generate beneath the silt seam reducing the shear resistance along the slip plane tremendously. Displacement time histories of representative points designated in Fig.3 (a), (d) are shown in Fig.3 (c), (f). In Case1, major displacement occurs mostly during shaking, while in Case2, post-shaking flow displacement is as large as that during shaking. Only upper sand layer moves again discontinuously along the silt seam after shaking. Note in Fig.3 (e) that the amount of displacement of upstream side is lager than that of down stream side. The flow along the water film causes the compression in the upper layer because the displacement is restricted at the down stream end by the soil container.

In Case 3-5, the confinement by the soil box is removed by truncating the edges of upper sand layer in the upstream and downstream sides as shown Fig.4 (d). In Fig.4, the displacement time histories of

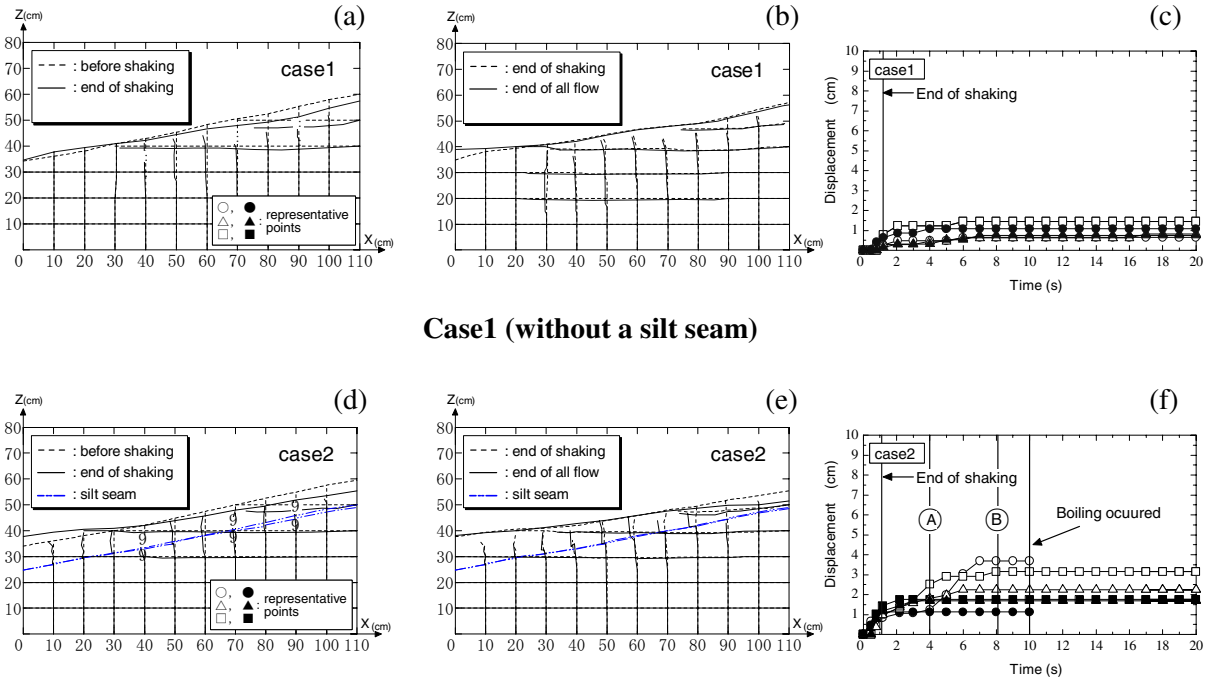

Case1 (without a silt seam)

Case2 (with a silt seam)

Fig.3 Deformation of sand slope: during shaking（a, d）and after shaking（b, e）and time history of displacement of representative points（c, f）.

representative points are shown. In Case 3, large displacement [Fig.4 (a)] due to water film effect occurs in the upper sand layer because of the unconfined flow in the down-slope direction. In Case4, displacement [Fig.4 (b)] is very little because of the absence of the silt seam, small shaking and gentle slope. However in Case 5 with a silt seam, though the test condition is almost the same as Case 4, the displacement of the upper sand layer [Fig.4 (c)] is much larger and the post-shaking flow takes place despite the gentleness of the slope.

It is easy to understand from the above test results that the flow due to water films is very much influenced by boundary conditions on the down slope side. If the down-slope side is confined, the flow displacement takes the compression mode in the upper layer. Even if the slope angle is only a few degrees, large flow displacement induced by the water film effect can occur.

Now, there may be a question that if shear strain of sand beneath a silt seam increases with increasing lateral flow in the upper sand layer, why the water film will not be absorbed by the dilation of the sand skeleton. In order to discuss this problem based on the experimental facts, it is very important to know the volume change of sand

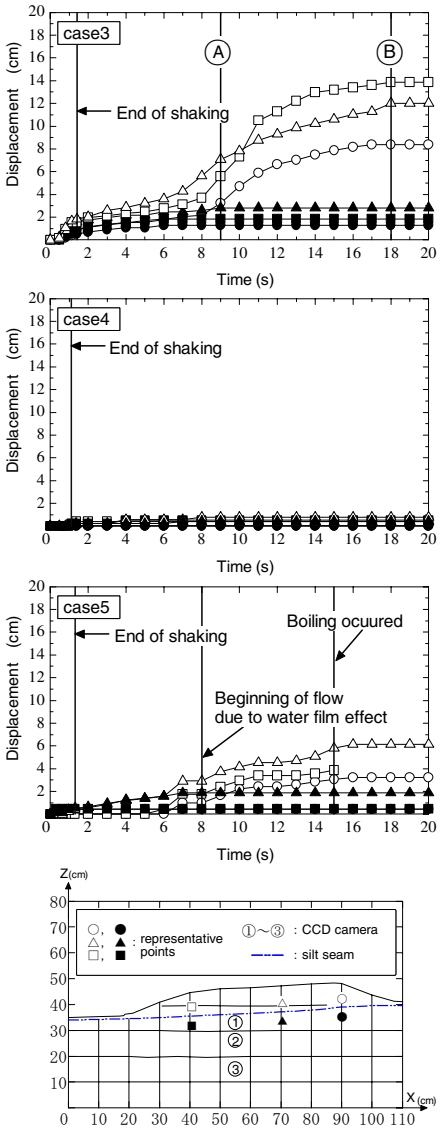

Fig.4 Displacement records of Case3-5.

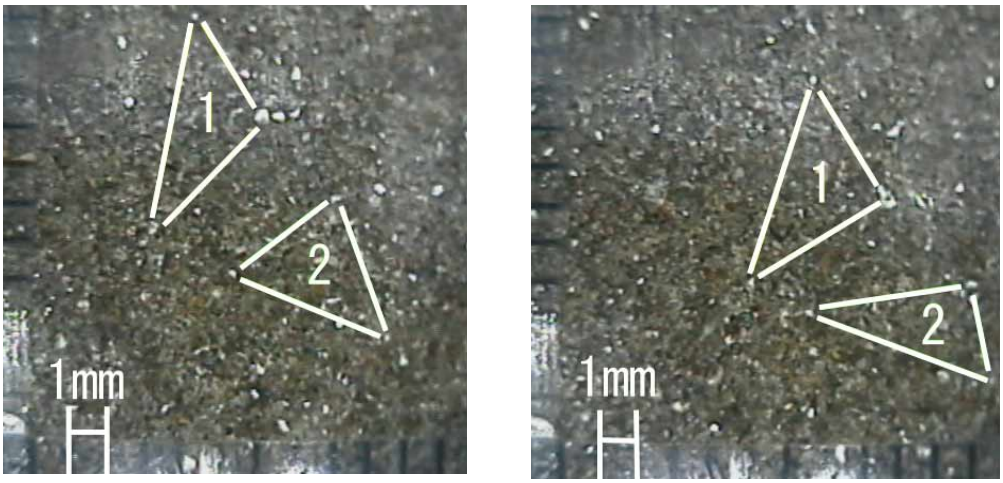

T= 1.3s (end of shaking) **T=15s**

Fig.5 Picture of volume change of sand (Case5, CCD1).

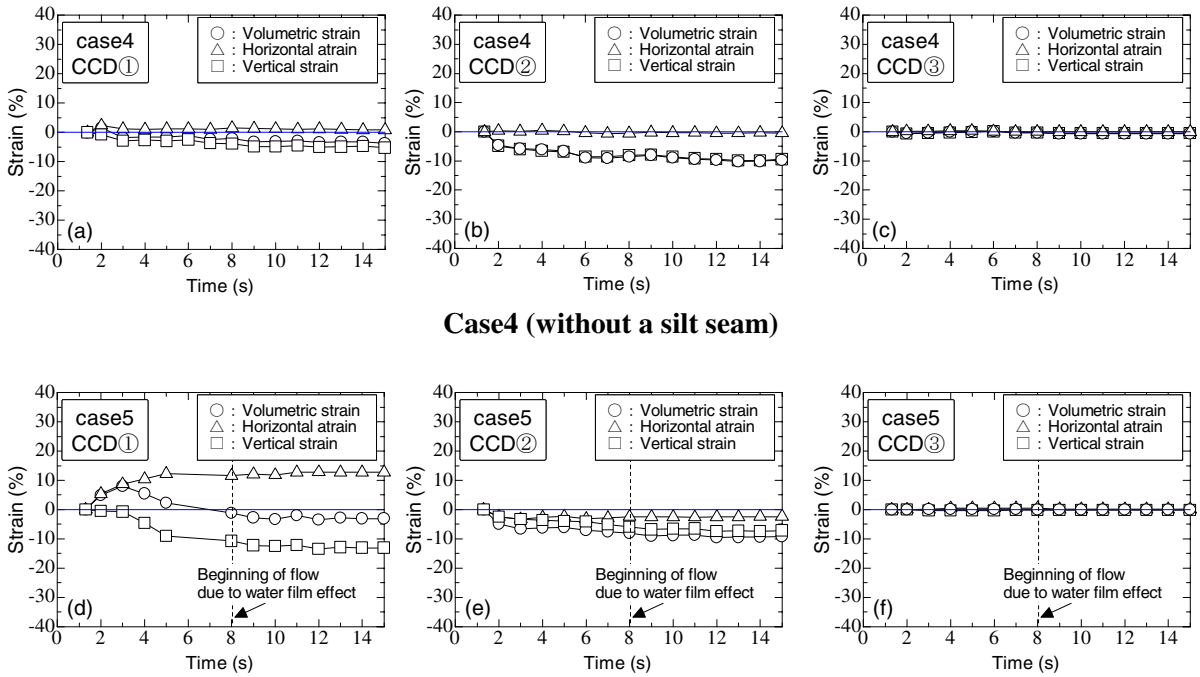

Case4 (without a silt seam)

Case5 (with a silt seam)

Fig.6 Time histories of strain after shaking in Case4 and Case5.

beneath the silt seam after shaking. Therefore, special efforts are made in this research to measure the volume change of sand by using CCD cameras. The locations of the cameras are indicated in Fig.4 (d). In Fig.5, the pictures taken at two time points are shown as examples. In order to measure the volume change from the pictures, five virtual triangles are drawn as indicated in Fig.5 by connecting randomly selected fifteen soil grains in the pictures taken by the CCD cameras. The coordinates of the 15 soil grains comprising five triangles are consecutively measured from which the volumetric strains are calculated as a sum of the vertical and horizontal strains. Fig.6 shows time histories of horizontal and vertical strains and volumetric strains. All the strains are evaluated as the mean values of the five triangles. There are extreme dispersions of the measured strain in CCD1 and CCD2 actually. As an example by CCD1 in case5, the volumetric strain of triangle 1 increases by 12%, while that of triangle 2 decrease by 13% in the time interval of T= 1.3 - 15 s as shown in Fig.6.

In Case4 without a silt seam shown in Fig.6 (a), the volumetric strain contracts slightly presumably because the deformation of the slope is so small as indicated in Fig.4 (b). On the other hand, in Case5 with a silt seam shown in Fig.6 (d), horizontal strain is disposed to dilation while the vertical strain is disposed to contraction, resulting in the increase in volumetric strain a few seconds after shaking as the amount of flow increases. The volumetric strain changes into contraction after 8 seconds which corresponds to the beginning of the flow due to the water film effect in the upper layer. In spite of large lateral flow as demonstrated in Fig.4 (c), the dilation of the sand is not observed in Fig.6 (d). At the location of CCD2 as shown Fig.6 (b) and (e), horizontal strain doesn't develop and vertical strain tends to be contractive in both cases. At the location of CCD3, both horizontal and vertical strains show minimal variations resulting in literary no volumetric strain.

ENERGY ANALYSIS FOR RESIDUAL STRENGTH ALONG WATER FILM

In Case2 & Case3, the residual shear strength exerted along the water film during the flow is calculated by the energy balance of the upper sand layer above the water film. In Fig.3 (f) and Fig.4 (a), the potential and kinetic energies at A and B are denoted as $E_{PA,}$ E_{KA} and $E_{PB,}$ $E_{KB,}$ respectively. In addition, the energy loss by friction between A and B is denoted as W. Therefore the energy balance is expressed as following;

$$E_{PA} + E_{KA} = E_{PB} + E_{KB} + W$$

then,

$$(E_{PA} - E_{PB}) + (E_{KA} - E_{KB}) = E_P + E_K = W \qquad (1)$$

Eq. (1) indicates that the change in the potential energy and the kinetic energy is equal to the energy loss during the flow between A and B.

In order to numerically evaluate Eq. (1), the upper sand layer is divided into n (n=9~10) blocks. For each block, the height of the center of gravity h_i of i'th segment is measured from video pictures at each time increment. Then, the potential energy change is evaluated from the change in h_i, buoyant mass M_i and gravity the acceleration of the gravity g for each block. Consequently, the change of potential energy during Point A to Point B is formulated as;

$$E_P = \sum_{i=1}^{n} M_{Ai}' g h_{Ai} - \sum_{i=1}^{n} M_{Bi}' g h_{Bi} \qquad (2)$$

Next, the change in the kinetic energy between Point A to Point B is expressed as

$$E_K = \frac{(\sum_{i=1}^{n} M_{Ai} v_{Ai}^{\,2} - \sum_{i=1}^{n} M_{Bi} v_{Bi}^{\,2})}{2} \qquad (3)$$

where v_i = velocity of soil mass of i'th segment.

It is assumed here that energy loss W in Eq. (1) between Point A to Point B is constituted from W_1 to W_5, where W_1= energy loss by friction along the water film, W_2 =energy loss by the friction between the sand and the wall of the soil box on both sides, W_3, W_4 =energy loss by the volumetric strain and shear strain in the flowing soil mass above the water film and W_5 =energy loss by viscosity of water in the water film. They are expressed as;

$$W_1 = \tan\phi' s\sum_{i=1}^{n}(\delta_i'\cos\theta_i A_i) \quad (4)$$

$$W_2 = s\sum_{i=1}^{n} 2\frac{\delta_i'}{2} l_i \mu K_0 B_i \quad (5)$$

$$W_3 = \sum_{i=1}^{n}\frac{1}{2}(\delta_{xi}'\varepsilon_{xi} + \delta_{yi}'\varepsilon_{yi})V_i \quad (6)$$

$$W_4 = \sum_{i=1}^{n}\frac{1}{2}(\tau_{xyi}\gamma_{xyi})V_i \quad (7)$$

$$W_5 = \mu_W \frac{\Delta v_{Aav}}{\Delta d} s\sum_{i=1}^{n} A_i \quad (8)$$

respectively, where ϕ' = equivalent friction angle in terms of effective stress, s = flow displacement tangent to the slip surface assumed constant, δ_i' = effective stress of the i'th segment, θ_i = gradient of the i'th segment bottom, A_i = bottom area of the i'th segment, l_i = height of the i'th segment, μK_0 = friction coefficient between sand and both sides of the acrylic soil container was also taken into consideration by using μK_0 =0.125, which had been experimentally obtained by a tube test carried out by Kokusho and Kojima [7], B_i = width of the i'th segment, δ_{xi}' = horizontal effective stress of the i'th segment, ε_{xi}' = horizontal strain of the i'th segment, δ_{yi}' = vertical effective stress of the i'th segment, ε_{yi}' = horizontal strain of the i'th segment, V_i = volume of the i'th segment, τ_{xyi}' = shear stress of the i'th segment, γ_{xyi}' = shear strain of the i'th segment, μ_W = viscosity coefficient of water is assumed 1.307mPa, v_{Aav} = average velocity of soil mass at A, d = thickness of water film is assumed 0.1mm. Here assuming that a soil deformation as elasticity.

Then, Eq (1) is expressed as

$$E_P + E_K = W_1 + W_2 + W_3 + W_4 + W_5 \quad (9)$$

The equivalent friction angle ϕ' in terms of effective stress during Point A to Point B can be calculated backward from Eq. (9).

The equivalent friction angle is calculated 3.88 degrees in Case 2 and 3.93 degrees in Case3. Fig.7 shows a relationship between the equivalent friction angle and relatively density. The star symbol indicates the angle of repose, ϕ' =29 degrees, measured by statically inclining the homogeneous sand slope [8] and the broken line indicated the

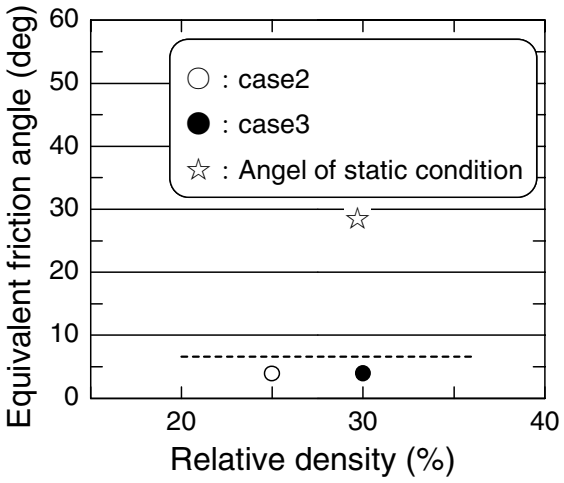

Fig.7 Equivalent friction angle versus relative density relationship

equivalent friction angle obtained in a series of model tests on slopes including an arc-shaped silt seam [9]. The average of the equivalent friction angle in that case was 6.6 degrees, corresponding to residual strength about 20% of that for a homogeneous slope. In this case, the residual strength along the slip surface beneath the silt seam decreases further to about 10% of that for a homogeneous slope. The difference in the reduction of equivalent friction angle may possibly be explained by the difference in the silt seam of arc and straight plane.

From results of the back calculation, equivalent friction angle is evaluated as non-zero value. This non-zero strength cannot be explained if the slip surface actually passes all through continuous water film. This is probably because the water film may be discontinuous or winding. More research is certainly needed to clarify the mechanism of residual strength mobilization along the slip surface just beneath silt seams.

CONCLUDING REMARKS

Model tests and energy analyses on lateral flow by water film effect in liquefied sand slope including silt seam have yielded the following major conclusions;

1) Flow failure due to water film effect causes compression in the displaced soil layer if the flow movement is restricted at the down-slope end.
2) If the down-slope end is free, large flow displacement can be induced by the water film effect.
3) From the pictures of CCD cameras, it has been demonstrated that the volume of sand just beneath a water film does not dilate so much in spite of large lateral flow and actually starts to contract when post-shaking flow occurs.
4) It is estimated that the residual strength along the slip surface beneath the straight silt seam considerably decreases to about 10% of that for homogeneous sand in contrast to 20% decrease for similar model tests of arc-shaped silt seam.

REFERENCES

1) Hamada, M., Yasuda, S., Isoyama, R. and Emoto, K. “Observation of permanent ground displacements induced by soil liquefaction” *Journal of Geotechnical Engineering, Japan Society of Civil Engineers,* No.376, Ⅲ-6, 221-220, 1986, (in Japanese).

2) Seed, H. B. “Design problems in soil liquefaction.” *Journal of Geotechnical Engineering, ASCE,* Vol.113, No.8, 827-845, 1987.

3) Dobry, R., Taboada, V., Liu, L. “Centrifuge modeling of liquefaction effects during earthquakes.” *Proc. of 1st International Conference on Earthquake Geotechnical Engineering, ASCE,* Vol.3, 1291-1324, 1997.

4) Castro, G. and Poulos, S.J. “Factors affecting liquefaction and cyclic mobility.” *Journal of Geotechnical Engineering,* Vol.103, No.6, 501-516, 1977.
5) Meneses, J., Ishihara, K., Towhata, I. “Effects of superimposing cyclic shear stress on the undrained behavior of saturated sand under monotonic loading.” *Soil and Foundations,* Vol.38, No.4, 115-127, 1998.
6) Kokusho, T. “Water film in liquefied sand and its effect on lateral spread., *Journal of Geotechnical and Geoenviromental Engineering, ASCE*, Vol.125, No.10, 817-826, 1999.
7) Kokusho,T. and Kojima,T. “Mechanism for Postliquefaction Water Film Generation in Layered sand.” *Journal of Geotechnical and Geoenviromental Engineering, ASCE*, Vol.128, No.2, 129-137, 2002.
8) Kabasawa, K. and Kokusho. T. “Possibility of water film generation in saturated sand slope subjected to static loading.” *Proc. Annual Convention of Japan Society of Civil Engineers*, Vol.3, 2001: 346-347, (in Japanese).
9) Kabasawa, K. and Kokusho. T. “Energy analysis and model tests on lateral flow induced by water film effect in liquefied ground.” *Journal of Geotechnical Engineering, Japan Society of Civil Engineers*, now printing, (in Japanese).